NASA-CR-201979

AIAA 94-1905
Three-Dimensional Navier-Stokes Simulations with Two-Equation Turbulence Models of Intersecting Shock-Waves/Turbulent Boundary Layer at Mach 8.3

J.E. Bardina,
MCAT Institute,
Sunnyvale, CA
T.J. Coakley,
NASA Ames Research Center,
Moffett Field, CA

12th AIAA Applied Aerodynamics Conference
June 20-23, 1994/Colorado Springs, Colorado

THREE-DIMENSIONAL NAVIER-STOKES SIMULATIONS WITH TWO-EQUATION TURBULENCE MODELS OF INTERSECTING SHOCK-WAVES/TURBULENT BOUNDARY LAYER AT MACH 8.3

J.E. Bardina*
MCAT Institute,
Sunnyvale, California

T.J. Coakley†
NASA Ames Research Center,
Moffett Field, California

Abstract

An investigation of the numerical simulation with two-equation turbulence models of a three-dimensional hypersonic intersecting (SWTBL) shock-wave/turbulent boundary layer interaction flow is presented. The flows are solved with an efficient implicit upwind flux-difference split Reynolds-averaged Navier-Stokes code. Numerical results are compared with experimental data for a flow at Mach 8.28 and Reynolds number $5.3 \cdot 10^6$ with crossing shock-waves and expansion fans generated by two lateral 15 fins located on top of a cold-wall plate. This experiment belongs to the hypersonic database for modeling validation. Simulations show the development of two primary counter-rotating cross-flow vortices and secondary turbulent structures under the main vortices and in each corner singularity inside the turbulent boundary layer. A significant loss of total pressure is produced by the complex interaction between the main vortices and the uplifted jet stream of the boundary layer. The overall agreement between computational and experimental data is generally good. The turbulence modeling corrections show improvements in the predictions of surface heat transfer distribution and an increase in the strength of the cross-flow vortices. Accurate predictions of the outflow flowfield is found to require accurate modeling of the laminar/turbulent boundary layers on the fin walls.

Introduction

The present investigation is a continuous research effort to develop, verify and applly two-equation turbulence models for three-dimensional compressible turbulent flows[1-8]. Two-equation turbulence models are simple, general, robust, and efficient for CFD applications on high speed flows. Their simplicity is mainly due to the eddy viscosity hypothesis; their generality is built on the use of transport equations to define turbulent velocity- and length-scale instead of algebraic definitions; their robustness is based on recent advances on numerical methods; and their efficiency is based on continuous improvements of present numerical processors. There is clear evidence showing that most widely used two-equation models tend to under-predict flow separation and over-predict heat transfer near flow re-attachment regions. In hypersonic flow calculations, these model deficiencies are even more pronounced, particularly regarding their inability to predict the extent of the flow separation.

In a recent investigation, Bardina and Coakley[1] tested two model corrections that were designed to remedy the above mentioned difficulties for 3-D hypersonic flows. Previously, Coakley and Huang[2] tested these model corrections against experimental data in 2-D compressible flows. The first one limits the turbulence length scale to be no greater than the von Kármán length scale. This correction is equivalent to the use of a one-equation model in regions where the length scale of the two-equation model is larger than the von Kármán length scale. The main effect of this correction was observed to reduce the heat transfer rate near flow-reattachment in agreement with experimental observations. The second model correction, designed to increase the extend of separation, causes the length scale to decrease (or increase) when the flow undergoes rapid compression (or expansion).

The development and validation of turbulence models for hypersonic shock-wave/turbulent boundary layer interactions is based on the fundamental understanding of the turbulence physics of the flows and the availability of an acceptable experimental database. In a parallel research effort to this investigation, Settles and Dodson[9-11] have completed an extensive review of the available experimental data on compressible turbulent high-speed flows suitable for turbulence model validation. This research was developed for the (NASP) National AeroSpace Plane program in the Modeling and Experimental Validation Branch at NASA Ames Research Center. The review of 2-D and 3-D flows includes complex hypersonic flows with pressure profiles, skin friction, wall heat transfer, yaw

*Senior Research Scientist.
†Research Scientist. Member AIAA.

angles, pitot pressure, and turbulence statistics data. In this paper, we present comparisons of numerical simulation results and the selected experimental data of Kussoy and Horstman[12] on intersecting shock-waves/ turbulent boundary layer (ISWTBL) interactions. This simple geometry shows complex turbulence structures of great interest in the design of uniform high-pressure flows at the entrance of inlets.

Turbulence Models

The turbulence models used in this study are the two-equation k-ω model of Wilcox[13,14], the k-ε model of Launder and Sharma[15], the SST (k-ω/k-ε) model of Menter[16] and the algebraic eddy viscosity model formulation of Baldwin and Lomax[17]. The two-equation k-ω model is also studied with the compressibility model corrections, in particular, the length-scale and the separation corrections. A detailed description of these models is found in the references, and a detailed description of these models, including the model corrections is found in references 2 and 4. The main aim of the present effort is to further study the effects of the compressibility corrections in the simulation of complex 3-D flows. Currently, research on improved compressibility corrections for turbulence modeling is being performed to account for the complex effects encountered in shock boundary layer interactions.

Numerical Method

The cost-effective engineering design of aerospace vehicles encountering subsonic, transonic, supersonic and hypersonic speeds requires advanced and efficient computational fluid dynamics (CFD) technology[8]. Accurate aerodynamic prediction of complex full 3-D flow fields and the integration of different areas of technology and research are presently required to account for the significant nonlinear effects on aerodynamic coefficients, lift, drag, and heat load. An improved 3-D Navier-Stokes code has been further developed to efficiently validate turbulence models for high speed flows. The general methodology is found in Bardina[3], and therefore only a brief description of the method is given below.

The model equations are the 3-D compressible Reynolds-averaged Navier-Stokes equations Turbulence Models in a general curvilinear coordinate system with mass-averaged and non-dimensional variables. All flux differences are treated implicitly in order to increase stability and to be able to use large increments of time or CFL numbers. The numerical scheme for the viscous fluxes is second-order central difference, while the numerical scheme for the inviscid fluxes is a higher-order TVD upwind flux-difference splitting. The higher-order TVD scheme has the capability to represent first-order upwind, second-order upwind, third-order upwind biased, second-order Fromm scheme, and other combinations of second-order upwind and central differences.

The efficiency of the method is based on an implicit symmetric Gauss-Seidel "method of planes" relaxation scheme with alternating directional space marching sweeps along one coordinate direction, Newton-Raphson inner iteration procedure with an implicit block-tridiagonal diagonally dominant approximate factorization relaxation scheme along the other two directions. This method requires less data in central memory and less total transfer of data into central memory per iteration than implicit upwind schemes using only time-dependent approximate factorizations; therefore, the capability of processing larger and/or complex data bases and computational grids is available. The data is conveniently stored on successive planes along the streamwise coordinate, and the system of equations is solved twice in each successive plane first along the forward direction and afterwards along the backward direction. The repeated solution procedure provides an effective Newton-Raphson convergence acceleration. In each plane the solution is obtained by a two level diagonally dominant approximate factorization DDADI procedure[13]. The space marching alternating directional sweeps in the streamwise coordinate are von Neumann unconditionally stable for zones of subsonic and streamwise separated and reversed flows as well as supersonic flow. As the more restrictive PNS techniques, the present space marching method results in improved propagation of nonlinear effects to accelerate convergence to steady state, generally in about one order of magnitude fewer iterations than approximated factorization methods.

This method combines the best features of data management and computational efficiency of space marching procedures with the generality and stability of time dependent Navier-Stokes procedures to solve flows with mixed subsonic and supersonic zones, including streamwise separated flows. Its robust stability derives from a combination of conservative implicit upwind flux difference splitting, inner approximation procedure in grid cells where changes of eigenvalue sign are present, diagonally dominant approximate factorization and relaxation scheme, flux limiters of higher-order flux differences, and well-posed characteristic-based implicit boundary approximations. It provides the capability of predicting complex flow structures in complex geometries with good accuracy.

Boundary Conditions

Mathematically well posed implicit characteristic-based boundary procedures were imposed at every boundary point. The equilibrium turbulent boundary layer was prescribed at the inflow boundary points. The inflow profile matched the experimental displacement thickness, δ^*_∞=0.0126 m, located at 1.62 m from the leading edge of

the flat plate. On the fin and flat plate boundary points, constant wall temperature (T_w=300 °K) and no slip conditions were imposed; the turbulent kinetic energy k and its dissipation rate ε were set equal to zero; ω was set equal to 10 times greater than the corresponding theoretical value at the first point off the wall. On the symmetry plane, no flow through and zero-gradient extrapolation of density, pressure, streamwise velocity, and turbulence variables were imposed. On the upper free-flow plane and other inflow/outflow boundary points, finite difference was imposed both along and toward the boundaries. The procedure automatically determined whether the fluid was flowing locally toward or fromm the boundary, and it imposed appropriate conditions accordingly. If the inflow was subsonic, no changes in entropy, tangential velocity components, enthalpy, and turbulence variables were imposed. If the outflow was subsonic, no pressure gradient was imposed since only one characteristic-based boundary approximation was required in the differences toward the boundary. If the outflow was supersonic, the solution was naturally extrapolated with the upwind scheme with no external boundary approximations. These boundary approximations have been proven to be effective in previous simulations and free stream has been effectively maintained[3].

Code Performance

The numerical simulations in the Cray Y-MP C90 supercomputer located at NASA Ames Research Center performed at a rate of 51 MIPS and 288 MFLOPS. Simulations studies were done with 101x61x41 and 231x81x81 grid points. Small differences between the solutions were observed in the surface pressure and heat transfer distributions, more differences were observed in the flow structures. The fine mesh solutions provided the best resolution of the turbulence structures, while the less refine mesh solutions are considered accurate for engineering purposes. Most results presented here were obtained with the 101x61x41 grid and required less than 6 hours of CPU time and less than 600 sweeps (or global iterations) to achieve convergence to steady state. The performance of this diagonal-dominant implicit upwind code shows at least one order of magnitude better efficiency than other Navier-Stokes codes based on well-known central-difference numerical methods.

Intersecting Shock-Waves/Turbulent Boundary Layer Interaction (ISWBLI)

The Ames experiment of Kussoy and Horstman[12] on 3-D shock-wave boundary-layer interactions was used here to test the compressible turbulence models and the model corrections. This experiment studies the interactions of two intersecting hypersonic shock waves with a thick turbulent boundary layer. The experimental configurations reflect several key elements of generic hypersonic inlets, thick turbulent boundary-layer approaching two vertical fins of varying wedge angles, crossing shock-waves, boundary-layer cross-flow vortices, and large pressure gradients. The test body for this series of experiments is shown in fig.1. Two 15° fins mounted on top of a 2.2 m long flat plate generated two planar oblique crossing shock waves on a thick turbulent boundary layer. The free-stream Mach number was M_∞ = 8.3, the free-stream temperature was T_∞ = 80 °K, the Reynolds number was $Re_\infty = 5.3 \cdot 10^6$ per meter, and the wall temperature was fixed at 300 °K.

The physics of this flow shows a pattern of intersecting shock-waves above the boundary layer and a complex set of cross-flow vortices and structures inside of the turbulent boundary layer. Previous experimental and computational analyses have provided a general description of the flow fields generated through the interaction of a single shock-wave and a turbulent boundary layer. Settles and Dolling[18] reviewed the early work on this class of turbulent flow interaction, while Kubota and Stollery[19] described the main vortical structure developed inside the boundary layer and under an oblique shock-wave. The interaction of each shock wave with the boundary layer generated a cross-flow vortex separation with a "quasi conical" shape[1,20,21]. Although the "quasi-conical" structure has been used in different studies of turbulence models and conical simulations[21,22], this approximation has been disputed previously[1]. The comparison of Bardina et al[1] and Knight et al[21] shows that this approximation introduces large errors and make comparisons of turbulence models meaningless. In this particular experiment, the influence of the lateral fins in the flow structures and surface quantities imply the necessity of a full 3-D numerical simulation. This flow is further complicated by the intersection of both counter-rotating cross-flow vortices, which uplifted the flow, producing large losses of total pressure, and generating a very complex flow structure with secondary structures developed under the cross-flow vortices and on the lateral fins. The fins developed their own hypersonic laminar boundary layer with expansion fans and lateral separation. In recent numerical investigations, Narayaswami et al[23] used the algebraic mixing-length model of Baldwin and Lomax, and the modified k-ε model of Rodi[22] for the turbulent eddy viscosity. Their results showed qualitative agreement with experimental data, peak surface pressures and heat transfer data are overpredicted. Gaitonde and Shang[24] have used the Baldwin and Lomax turbulence model and Roe's flux-difference split upwind numerical scheme. Their results show agreement with surface pressure data, and overprediction of surface heat transfer data.

A selected comparison between experimental data and numerical simulation results is described below. In general, symbols in the figures shown below represent the experimental data points, the solid lines show solutions

obtained with two-equation turbulence models, and the dash lines show solutions obtained with two-equation turbulence models and model corrections (length-scale and rapid compression corrections).

Velocity vectors

A set of velocity vector plots are shown in Figure 2. These results were obtained with the k-ω model including the length-scale and rapid compression corrections. The fin boundary layers were treated as turbulent below and laminar above the edge of the flat-plate boundary layer. Fig. 2a shows the velocity vectors next to the flat plate surface. It shows the vortex interaction zone, the flow turning and reflections, and the wake-like structure in the downstream zone. Fig. 2b shows the velocity vectors in the symmetry plane between the lateral fins. The main results show the uplifting of the boundary layer flow due to the vortex "collision", and the secondary uplifting and reattachment below the main vortices. Fig. 2c, 2d,2e, and 2f show velocity vectors in different crossed sections, x/δ_∞ = 3, 6, 9, and 12, respectively. They show the formation of two cross-flow vortices as main structures, a center bubble under the main vortices, corner vortices in the fin/plate junctions, and strong flow turnings at the edge of the flat plate boundary layer. The strength of the main vortices is model dependent. Figures 2f, 2g, and 2h compared the standard k-w model with and without model corrections and modeling the fin boundary layer as turbulent/laminar, turbulent, and laminar, respectively. The main feature is the increase of vorticity generated by the model corrections (Fig. 2f and 2h) and the almost disappearance of the main vortices with the standard k-ω model (Fig. 2g).

Pressure contours

Figures 3a and 3b show the normalized pressure contours in two cross-section planes. It shows the well known structure of the "quasi-conical" shape, the vortex, the triple point, the slip line. In the center zone, a secondary structure on the plate surface and a pressure wave between the plate surface and the free stream are present. These features show the complexity generated by the double fin interaction, beyond the single fin case.

Flow-field yaw angle

Figures 4a through 4e show the comparison of yaw-angle contours between simulation and experiment on different cross-sectional planes. The main emphasis is to differentiate between the simulations with and without model corrections, and to verify if the treatment of the fin boundary layers affect the results. The flow turning as represented by the yaw-angle is well modeled with the model corrections in Fig. 4b and 4e, especially if we consider the few measurements available in each plane. On the other hand, the absence of the model corrections in Fig. 4d shows almost no turning above the main vortices as shown in the experimental data.

Flow-field pitot pressure

Figures 5a through 45 show the comparison of Pitot pressure contours between simulation and experiment on different cross-sectional planes. The main emphasis is also to differentiate between the simulations with and without model corrections The low Pitot pressure zone in the main vortices zone shows agreement with the experimental data, especially if we consider the few experimental measurement points in each plane. The model corrections show larger gradients in Fig. 5b than the simulations without the model corrections in Fig. 5d. The laminar treatment of the fin boundary layers shown in Fig. 5e shows large differences with the turbulent/laminar treatment shown in Fig. 5b.

Surface pressure

Figure 6 shows the comparisons between prediction and experimental data of surface pressure distributions on the flat plate. Fig. 6a shows the centerline profiles between the two lateral fins. Figures 6b, 6c, and 6d show transverse surface pressure distributions at x/δ_∞ = 5.6, 6.92, and 8.31 boundary layer thicknesses downstream of the fin leading edges, respectively. A wave structure with high and low peaks of static pressure are observed. The pressure rises induced by the shock waves generated by the fin leading edges, and decreases induced by the expansion fans generated by the interior fin corners. The peak pressure value is located at the reattachment zone of the secondary structure formed under the two principal counter-rotating vortices. The first transverse distribution is located in the shock-wave "collision" zone, the second one is located near the peak surface pressure zone generated by the secondary flow re-attachment, and the third one is located near the lower expansion pressure zone. The turbulence models shown here are the k-ω model, the SST model and the Baldwin-Lomax model. The k-ω model includes the (l) length-scale, (r) separation bubble, and/or (w) rotation corrections. All simulations show good agreement with the experimental data, and the peak values are well predicted within the experimental uncertainty of 10%. Overprediction near the outflow zone is observed when the fin boundary layer are computed as (tur) turbulent boundary layers. If the fin boundary layers are computed as (lam) laminar boundary layers, no overprediction is obtained. The best treatment is obtained when the fin boundary layer is treated as (tur/lam) turbulent below and laminar above the turbulent boundary layer on the flat plate. Different from the results observed with a single fin[1], the modeling of the fin boundary layers affect the centerline pressure distribution. Since the pressure ratio in this 3-D simulations is smaller than the ones presented in the 2-D hypersonic database experiments[9-11], the model corrections show only small differences in the numerical predictions.

Surface heat transfer rate

Figure 7 shows the comparisons between prediction and experimental data of surface heat transfer distributions on the flat plate. Similar to the pressure distributions shown in the previous figures 6, Fig. 7a shows the centerline distributions and Figures 7b, 7c, and 7d show the transverse distributions at x/δ_∞ = 5.08, 6.4, and 7.78, respectively. A similar wave structure with high and low peaks along the centerline is also observed. The experimental data in the transverse profiles show a flatter distribution in the cross-sectional planes. Recent

simulations of Narayanswami et al[23] and Gaitonde et al[24] showed overprediction of heat transfer rate and "are thought to be associated with deficiencies in turbulence modeling." Therefore, the testing of the turbulence model corrections is of great interest here.

All models showed excellent agreement with the experimental data along the centerline distribution. The small plateau at the beginning of the interaction is not shown in this 101x61x41 grid simulations, however, they are present in the 231x81x81 simulations not shown here. In the transverse distributions, the k-w, SST, and Baldwin-Lomax models show an overprediction which seems to be associated with the cross-flow reattachment. The model corrections improve the predictions and show good agreement with the experimental data in the first two stations shown in Fig 7b and 7c. This agreement is only present when the fin boundary layers are treated as turbulent ones below the edge of the boundary layer on the flat plate. These results support the model corrections and the proper treatment of each boundary layer. Once again, best treatment is obtained when the fin boundary layer is treated as (tur/lam) turbulent below and laminar above the turbulent boundary layer of the flat plate. In the last transverse station shown in Fig. 7d, overprediction in the lateral cross-flow reattachment zone is still observed with all models, and it shows the complexity of this flow.

Total pressure

Figure 8 shows the normalized total pressure distribution along the streamwise direction. The numerical results[21] obtained by Horstman with Rodi's modified k-ε model and Knigth with the Baldwin-Lomax model are also included in this figure. The results show a significant loss of about 85% in total pressure due to the boundary layer interaction with the shock-waves forming the two cross-flow vortices as a low total pressure outflow jet. The need to eliminate these efficiencies in this kind of interaction is a subject of continuous research, including boundary layer bleeding and geometry modifications.

Concluding Remarks

In this section we summarize the research work, give our principal results and recommendations, and discuss plans for future work.The more promising turbulence model corrections for compressible flows were tested. The agreement with the experimental data is very good in surface pressure, heat transfer r rates, yaw angles, and Pitot pressure. The model corrections give improved heat transfer predictions. Different than the single fin simulations, The treatment of the fin boundary layer affects the surface plate predictions. The best results are obtained with the proper turbulent/laminar boundary layer on the fin walls. Accurate and efficient aerodynamic predictions of the intersecting SWTBL interaction have been presented. The present results show that numerical solutions can be efficiently obtained in order to provide a data set for engineering design. The flow structures are well captured within a few grid points and free of oscillations. The predictions in these zones are superior and show detailed primary and secondary turbulence structures. The physical understanding of these structures is fundamental to improve inlet designs and to improve the compressibility model corrections. This methodology provides a promising computational capability for aerospace vehicles.

Acknowledgments

This work is sponsored by NASA Ames Research Center, Modeling and Experimental Validation Branch, under Grant NCC 2-15. The authors wish to acknowledge helpful discussions with J.G. Marvin and C.C. Horstman.

References

1. Bardina, J.E., Coakley, T.J., and Marvin, J.G., "Two-Equation Turbulence Modeling for 3-D Hypersonic Flows," *AIAA-92-5064*, 4th International Aerospace Planes Conference, Orlando, Florida, December, 1992.

2. Coakley, T.J., and Huang,P.G., "Turbulence Modeling for High Speed Flows," *AIAA-92-0436*, Reno, NV, January 1992.

3. Bardina, J. E., "Three-Dimensional Navier-Stokes Method with Two-Equation Turbulence Models for Efficient Numerical Simulation of Hypersonic Flows," *AIAA-94-2950*, Indianapolis, IN, 1994.

4. Coakley, T.J., Horstman, C.C., Marvin, J.G., Viegas, J.R., Bardina, J.E., Huang, P.G., and Kussoy, M.I., "Turbulence Compressibility Corrections," to be published as NASA TM, 1994.

5. Coakley, T. J., and Marvin, J. G., "Compressibility corrections for Hypersonic Flow Turbulence Modeling," 1993 National Aero -Space Plane Technology Review, Monterey, CA, 1993.

6. Coakley, T. J., Huang, P. G., Bardina, J. E., and Viegas, J. R., "Modeling of Turbulence for Complex High Speed Flows," Second National Congress on Computational Mechanics, Washington, D. C., 1993.

7. Huang, P. G., and Coakley, T. J., "Turbulence Modeling for Complex Hypersonic Flows," *AIAA-93-0200*, Reno, NV., January, 1993.

8. Marvin, J.G., "A CFD Validation Roadmap for Hypersonic Flows," published in AGARD-CP-514, *Theoretical and Experimental Methods in Hypersonic Flows*, Reference 17, 1993.

9. Settles, G. S, and Dodson, L. J., "Hypersonic Shock/Boundary-Layer Interaction Database," *NASA CR 177577*, 1991.

10. Settles, G. S., and Dodson, L. J., "Hypersonic Turbulent Boundary-Layers and Free-Shear Layer Database," *NASA CR 1776*, 1993.

11. Settles, G. S, and Dodson, L. J., "Hypersonic Shock/Boundary-Layer Interaction Database: New and Corrected Data," Dept. of Mech. Engrg., Penn State Univ., University Park, PA; also to be published as *NASA CR*, 1993.

12. Kussoy, M.I., and Horstman, K.C., "Intersecting Shock_Wave/Turbulent Boundary Layer Interactions at Mach 8.3," *NASA TM 103909*, 1992.

13. Wilcox, D.C., "A Half Century Historical Review of the k-ω Model," *AIAA-91-0615*, Reno, NV, January, 1991.

14. Wilcox, D.C., "Progress in Turbulence Modeling," *AIAA-91-1785*, Honolulu, HI, Jun,e 1991.

15. Launder, B.E., and Sharma, B.I., "Application of the Energy-Dissipation Model of Turbulence to the Calculation of Flow Near a Spinning Disk," *Letters in Heat and Mass Transfer*, Vol. 1, 1974, pp. 131-138.

16. Menter, F.R., "Zonal Two Equation k-ω Turbulence Models for Aerodynamic Flows," *AIAA-93-2906*, Orlando, FL, June 1993.

17. Baldwin, B.S., and Lomax, H., "Thin Layer Approximation and Algebraic Model for Separated Turbulent Flows," *AIAA-73-257*, 1973.

18. Settles, G.S., and Dolling, D.S., "Swept Shock/Boundary Layer Interactions: Tutorial and Update," AIAA-90-0375, Reno, NV, January, 1990.

19. Kubota, H., and Stollery, J., "An Experimental Study of the Interaction Between a Glancing Shock Wave and a Turbulent Boundary layer," J. Fluid Mech., 116, 1982, pp. 431-458.

20. Knight, D. D., Badekas, D., Horstman, C. C., and Settles, G. S., "On the Quasi-conical Flowfield Structure of the 3-D Single Fin Interaction," *AIAA J.*, Vol. 30, No. 12, 1992, pp. 2809-2816.

21. Knight, D.D., Horstman, C.C., and Monson, D.J., "The Hypersonic Shock Wave-Turbulent Boundary Layer Interaction Generated by a Sharp Fin at mach 8.2," *AIAA-92-0747*, Reno, NV, January, 1992.

22. Rodi, W., "Experience with Two-Layer Models Combining the k-ε with a One-equation Model near the Wall," *AIAA-91-0216*, Reno, NV, January, 1991.

23. Narayanswami, Horstman, C. C., and Knight, D. D., "Computation of Crossing Shock/Turbulent Boundary Layer Interaction at Mach 8.3," *AIAA-93-0779*, Reno, NV, January, 1993.

24. Gaitonde, D., and Shang, J.S., "Calculations on a Double-Fin Turbulent Interaction at High speed," *AIAA-93-3432*, Monterey, CA, August, 1993.

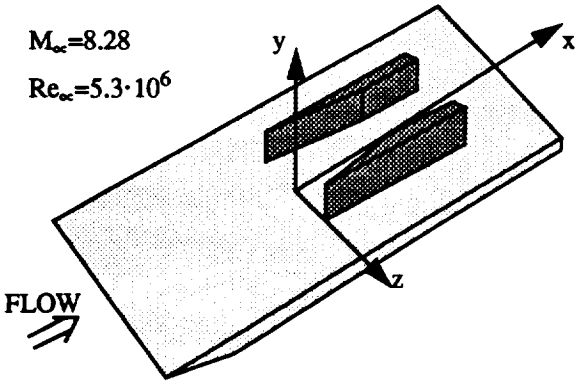

Fig. 1. Geometry of flat-plate with two 15° lateral fins.

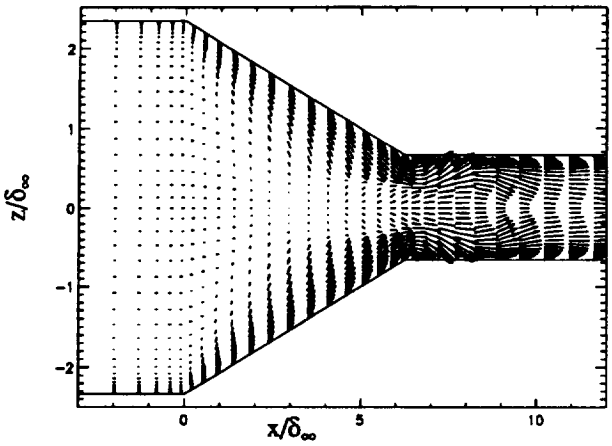

Fig. 2a. Velocity vectors on top of flat-plate surface. k-ω model with model corrections.

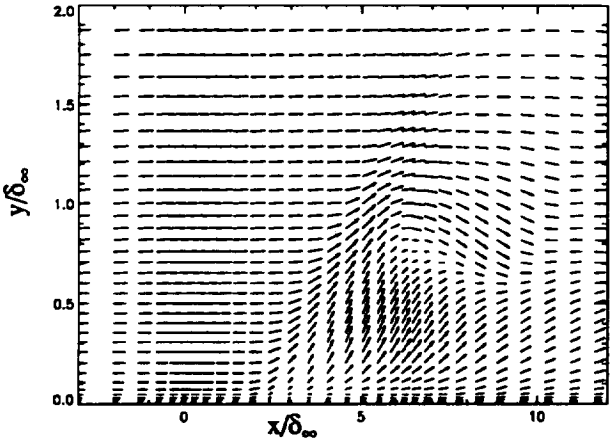

Fig. 2b. Velocity vectors on symmetry plane (Z = 0) between lateral turbulent/laminar boundary layer fins. k-ω model with model corrections.

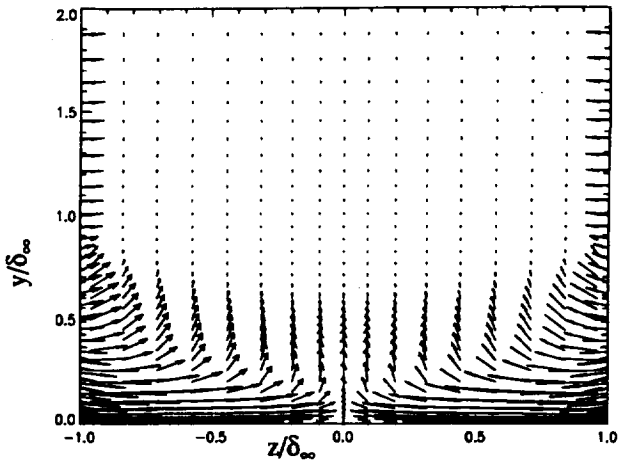

Fig. 2c. Velocity vectors on crossflow plane located at $x/\delta_\infty = 3$. k-ω model with model corrections.

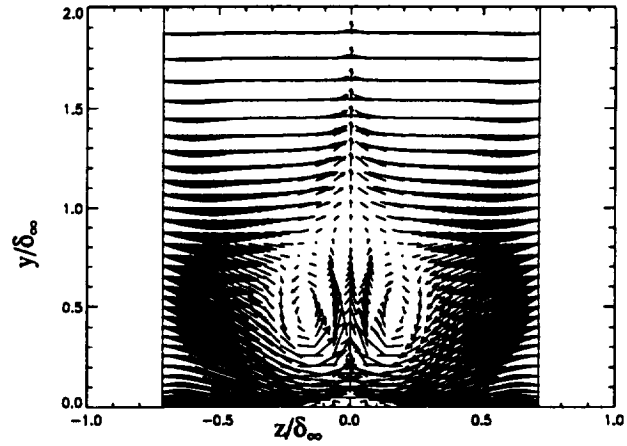

Fig. 2d. Velocity vectors on crossflow plane located at $x/\delta_\infty = 6$. k-ω model with model corrections.

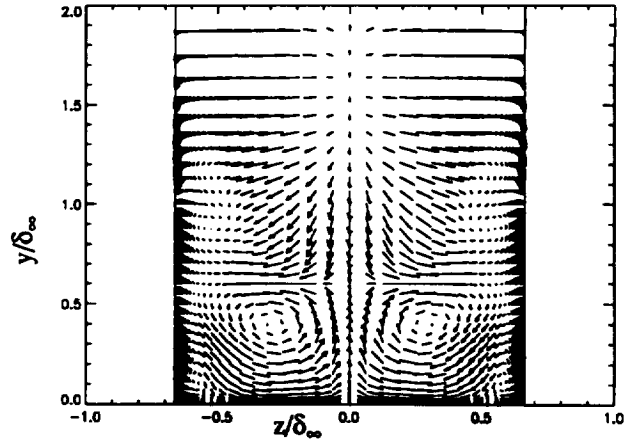

Fig. 2e. Velocity vectors on crossflow plane located at $x/\delta_\infty = 9$. k-ω model with model corrections.

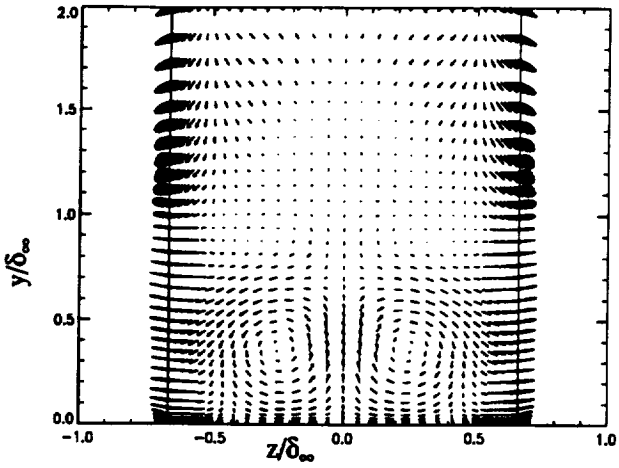

Fig. 2f. Velocity vectors on crossflow plane located at $x/\delta_\infty = 12$ and turbulent/laminar fin. k-ω model with model corrections.

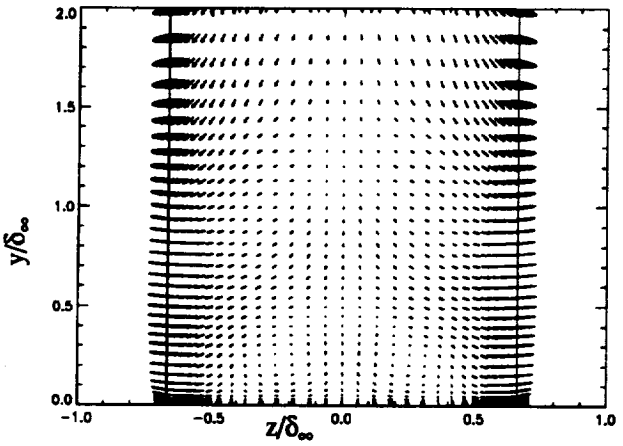

Fig. 2g. Velocity vectors on crossflow plane located at $x/\delta_\infty = 12$ and turbulent fin. k-ω model with no model corrections.

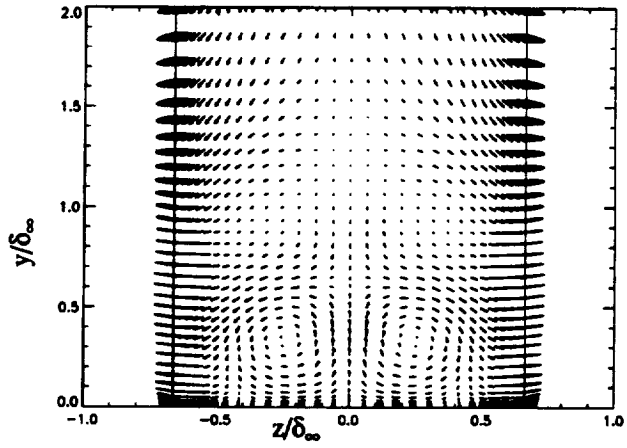

Fig. 2h. Velocity vectors on crossflow plane located at $x/\delta_\infty = 12$ and laminar fin. k-ω model with model corrections.

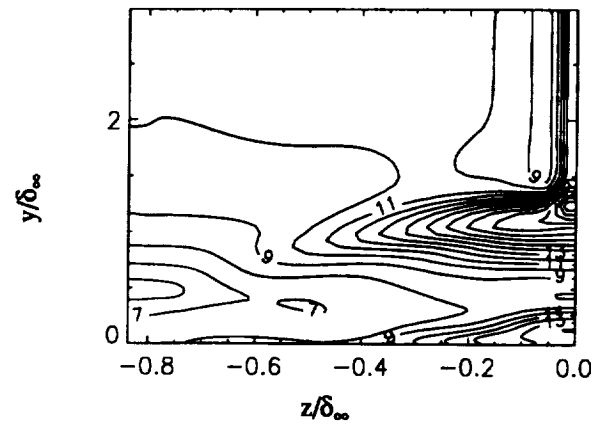

Fig. 3a. Normalized pressure contours on crossflow plane located at $x/\delta_\infty = 6$ and turbulent/laminar fin. k-ω model with model corrections.

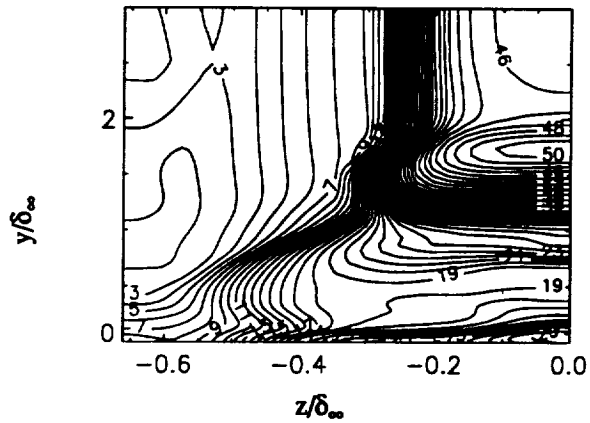

Fig. 3b. Normalized pressure contours on crossflow plane located at $x/\delta_\infty = 9$ and turbulent/laminar fin. k-ω model with model corrections.

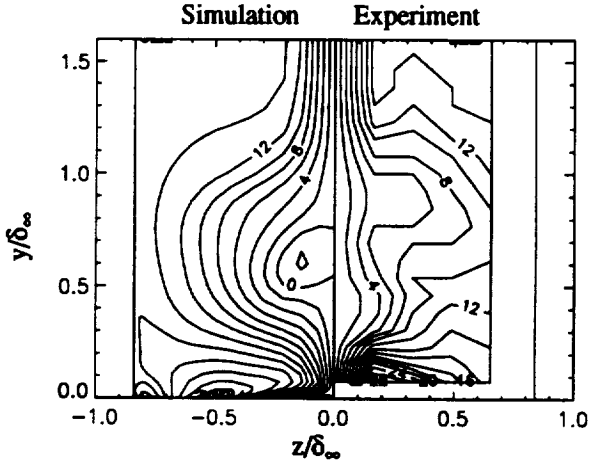

Fig. 4a. Yaw angle contours on crossflow plane located at $x/\delta_\infty = 5.6$ and turbulent/laminar fin with k-ω model and model corrections.

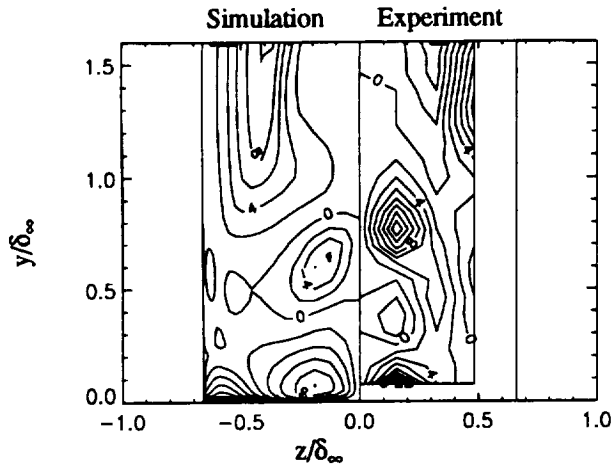

Fig. 4b. Yaw angle contours on crossflow plane located at $x/\delta_\infty = 6.92$ and turbulent/laminar fin with k-ω model and model corrections.

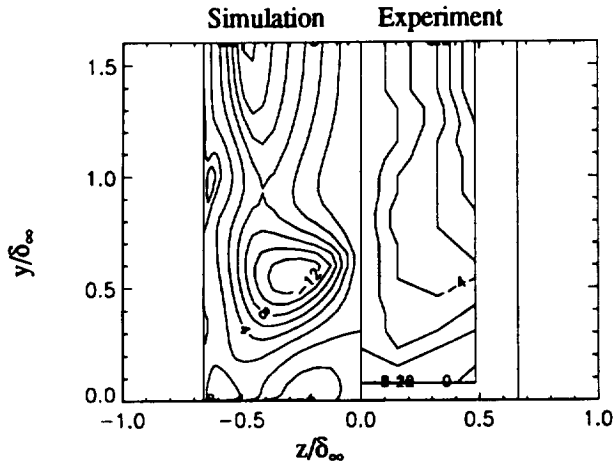

Fig. 4c. Yaw angle contours on crossflow plane located at $x/\delta_\infty = 8.3$ and turbulent/laminar fin with k-ω model and model corrections.

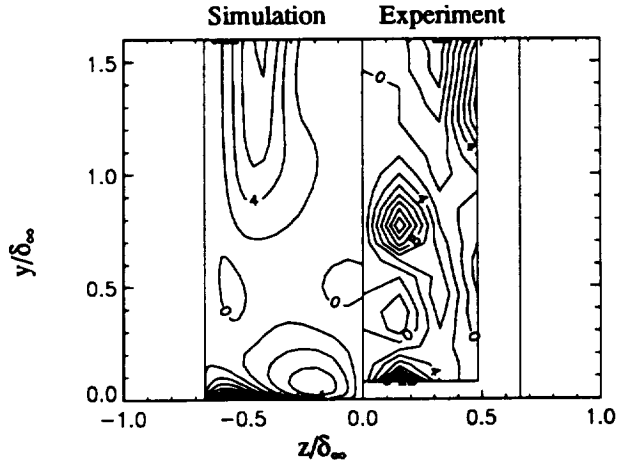

Fig. 4d. Yaw angle contours on crossflow plane located at $x/\delta_\infty = 6.92$ and turbulent fin with k-ω model and no model corrections

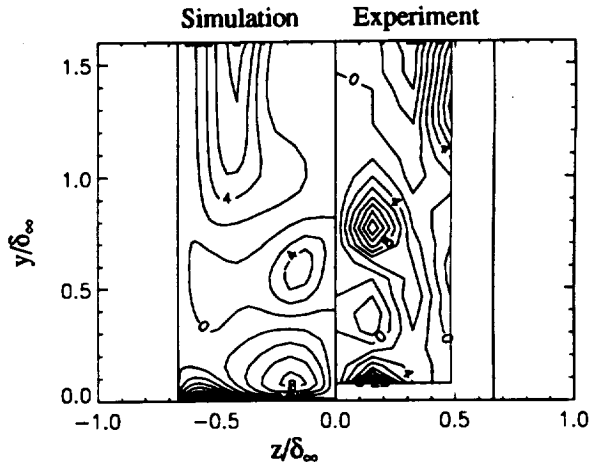

Fig. 4e. Yaw angle contours on crossflow plane located at $x/\delta_\infty = 6.92$ and laminar fin with k-ω model and model corrections.

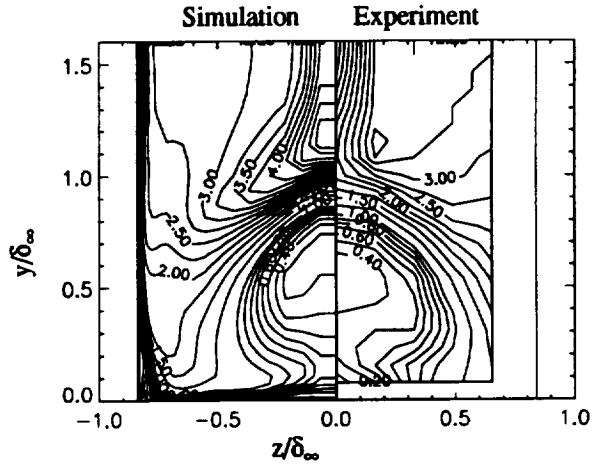

Fig. 5a. Pitot pressure contours on crossflow plane located at x/δ_∞ 5.6 and turbulent/laminar fin with k-ω model and model corrections.

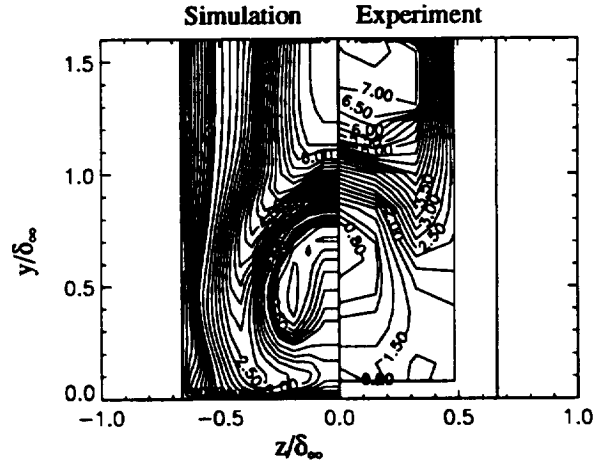

Fig. 5b. Pitot pressure contours on crossflow plane located at $x/\delta_\infty = 6.92$ and turbulent/laminar fin with k-ω model and model corrections.

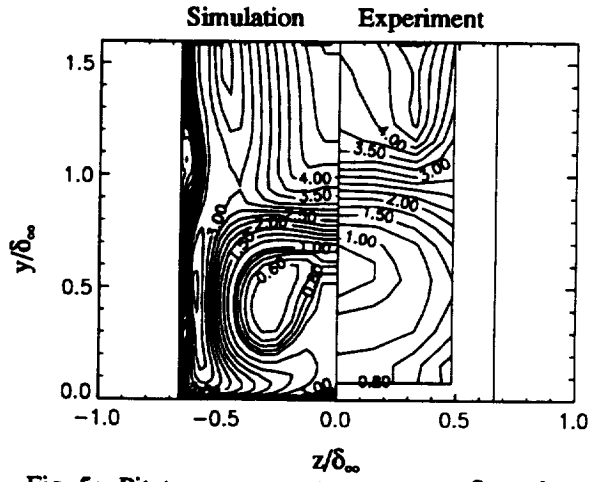

Fig. 5c. Pitot pressure contours on crossflow plane located at $x/\delta_\infty = 8.3$ and turbulent/laminar fin with k-ω model and model corrections.

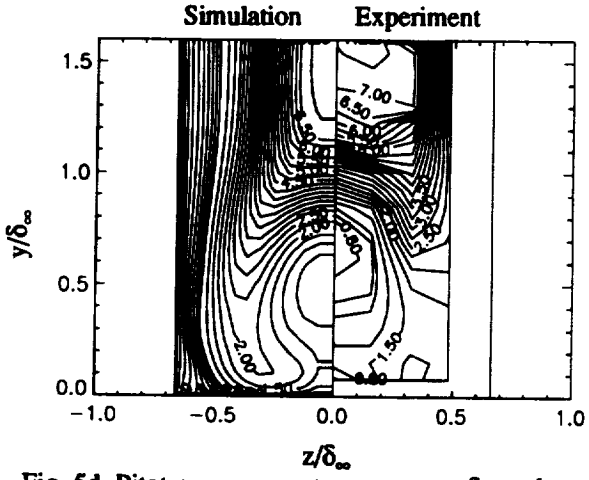

Fig. 5d. Pitot pressure contours on crossflow plane located at $x/\delta_\infty = 6.92$ and turbulent fin with k-ω model and no model corrections.

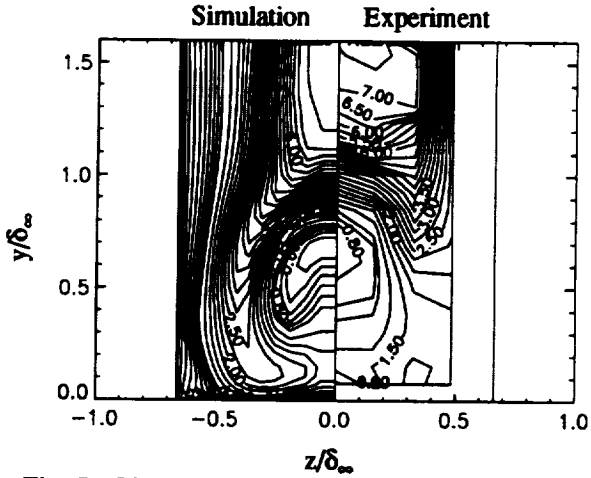

Fig. 5e. Pitot pressure contours on crossflow plane located at $x/\delta_\infty = 6.92$ and laminar fin with k-ω model and model corrections.

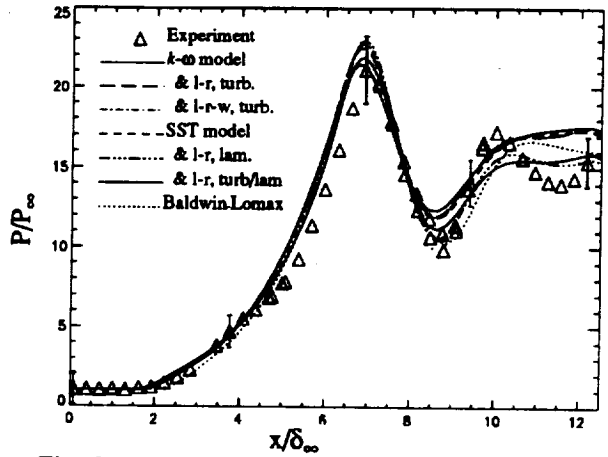

Fig. 6a. Normalized pressure distribution on centerline plane, $z/\delta_\infty = 0$ and $y/\delta_\infty = 0$.

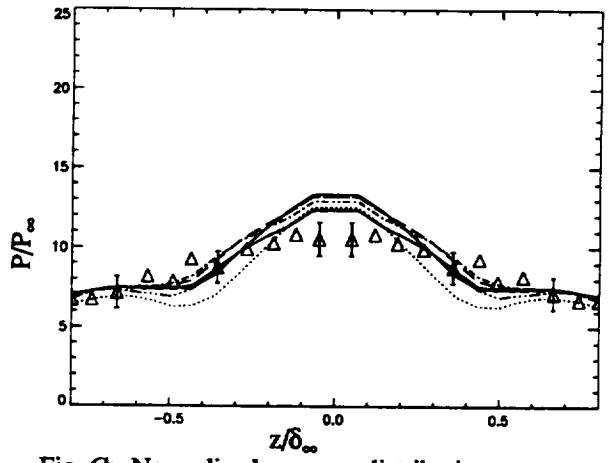

Fig. 6b. Normalized pressure distribution on crossflow plane located at $x/\delta_\infty = 5.6$ and $y/\delta_\infty = 0$.

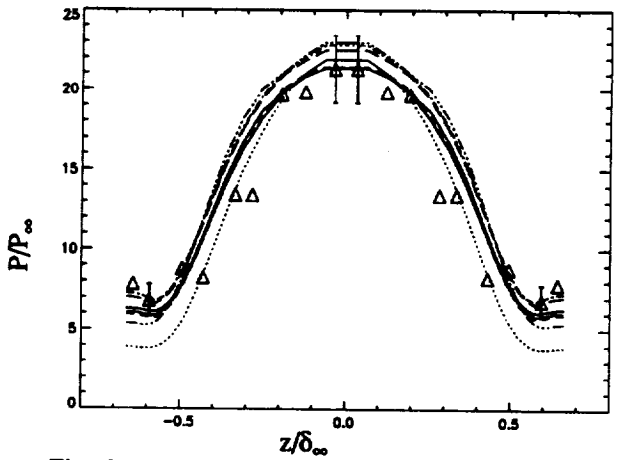

Fig. 6c. Normalized pressure distribution on crossflow plane located at $x/\delta_\infty = 6.92$ and $y/\delta_\infty = 0$.

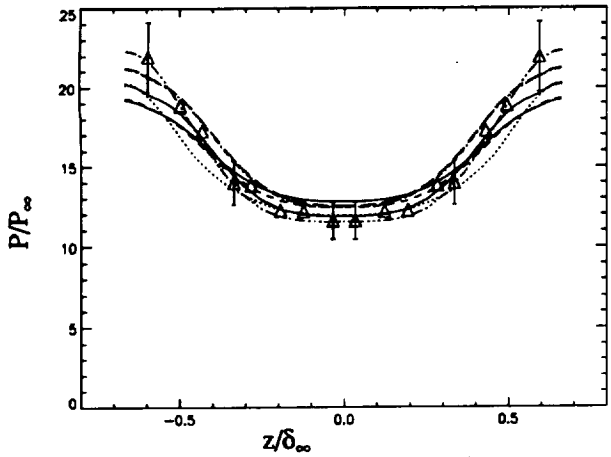

Fig. 6d. Normalized pressure distribution on crossflow plane located at $x/\delta_\infty = 8.3$ and $y/\delta_\infty = 0$.

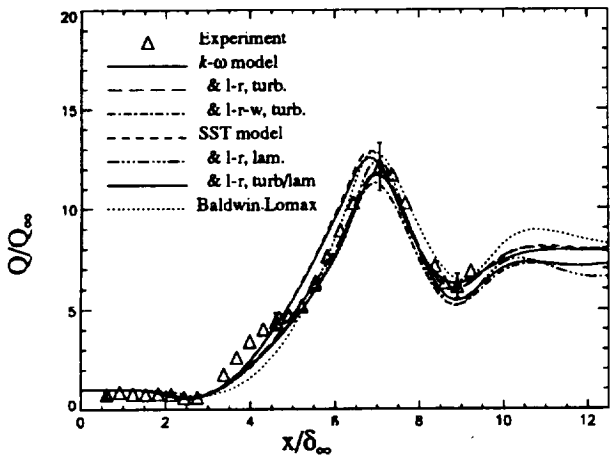

Fig. 7a. Surface heat transfer distribution on centerline plane, $z/\delta_\infty = 0$ and $y/\delta_\infty = 0$.

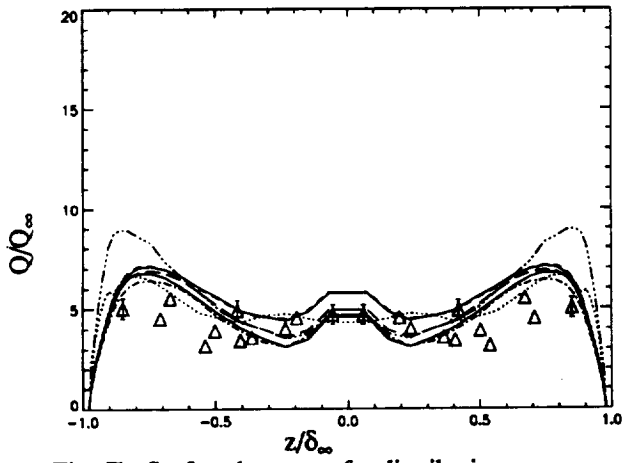

Fig. 7b. Surface heat transfer distribution on crossflow plane located at $x/\delta_\infty = 5.08$ and $y/\delta_\infty = 0$.

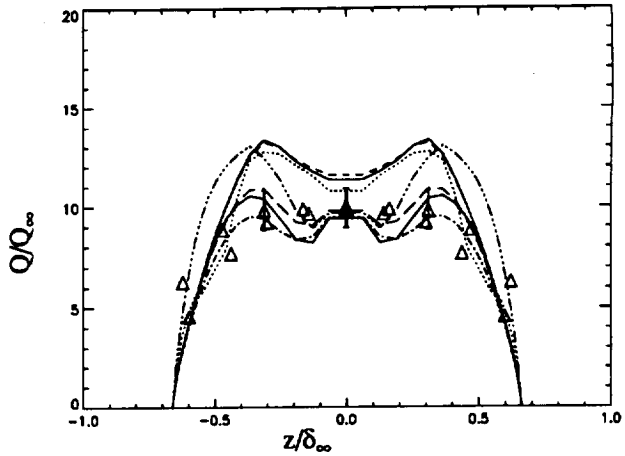

Fig. 7c. Surface heat transfer distribution on crossflow plane located at $x/\delta_\infty = 6.4$ and y/δ_∞

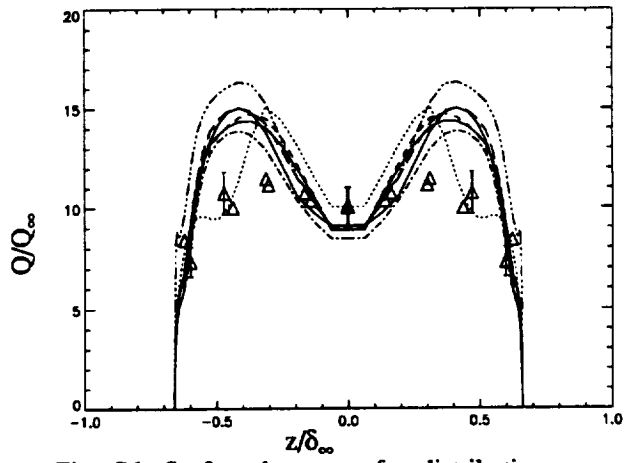

Fig. 7d. Surface heat transfer distribution on crossflow plane located at $x/\delta_\infty = 7.78$ and $y/\delta_\infty = 0$.

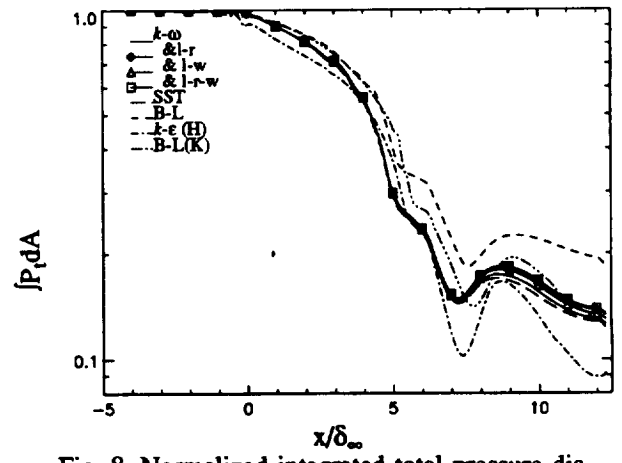

Fig. 8. Normalized integrated total pressure distribution.

NOTES